



# *Ex situ* studies of relaxation and crystallization in high-density amorphous ice annealed at 0.1 and 0.2 GPa

Includes response to: “Comment on: ‘Relaxation time of high-density amorphous ice’” by G.P. Johari

Philip H. Handle<sup>1</sup>, Markus Seidl, Violeta Fuentes-Landete, Thomas Loerting\*

Institute of Physical Chemistry, University of Innsbruck, Innrain 80-82, A-6020 Innsbruck, Austria



## ARTICLE INFO

### Article history:

Received 10 March 2016  
Received in revised form 12 April 2016  
Accepted 20 April 2016  
Available online 29 April 2016

### Keywords:

High-density amorphous ice  
Structural relaxation  
Crystallization rate  
Quench-recovery from high-pressure  
X-ray diffraction  
Differential scanning calorimetry

## ABSTRACT

In earlier work [P. H. Handle, M. Seidl and T. Loerting, *Phys. Rev. Lett.*, 2012, **108**, 225901] we reported on the relaxation time and extrapolated glass transition temperatures  $T_g$  of high-density amorphous ice (HDA) kept under a pressure of 0.1 and 0.2 GPa. Our *ex situ* strategy of obtaining these properties and the interpretation of our observations was recently assessed and questioned by Johari [*Thermochimica Acta*, 2014, **589**, 76–84]. Here we reply to the criticism, describe all our measurement and data analysis procedures in detail to reconfirm our earlier interpretation and conclusions. In addition to the more detailed analysis of relaxation times  $\tau_R$  we also present an analysis of crystallization times  $\tau_X$ . The comparison between the two reveals it is possible to significantly relax unannealed HDA (uHDA) at 0.1 and 0.2 GPa prior to its full crystallization.

© 2016 The Authors. Published by Elsevier B.V. This is an open access article under the CC BY license (<http://creativecommons.org/licenses/by/4.0/>).

## 1. Introduction

Water, the molecule of life, is very peculiar. The liquid that is composed of myriads of interacting H<sub>2</sub>O molecules shows very uncommon properties. Martin Chaplin currently lists 73 such anomalies [1]. It is known that several anomalies become more pronounced at low temperature [2]. An explanation of these anomalies was put forward through computer simulation work [3], namely the proposal of two distinct forms of liquid water at low temperatures. These two liquids differ in terms of density and are considered to be thermodynamically continuously connected with the experimentally known low-density amorphous ice (LDA) and high-density amorphous ice (HDA), respectively [3,4]. The latter form HDA, which we deal with in this study, was first produced experimentally in 1984 by pressure induced amorphization (PIA) of hexagonal ice at 77 K [5]. Yet, it is still controversial whether HDA is connected to a supercooled liquid [5–14] or whether HDA is related to crystalline material [15–23]. To understand metastable materi-

als in general, and HDA in particular, it is important to understand the influence of annealing procedures. The transition temperature of HDA → LDA at ambient pressure has been known to be dependent on the thermodynamic history of the samples for two decades [4]. The transition temperature is raised when PIA is performed at higher temperatures or when high-pressure annealing procedures are applied [4]. In principle each unique thermodynamic path leads to a differently strained form of amorphous ice, i.e., an infinite number of states is possible. However, there are only three different “phases” of amorphous ices to which any amorphous state of water may converge to after annealing at sufficiently high temperature as a function of pressure [24]. Here we focus on relaxation within HDA, which is the most stable form of amorphous ice in the pressure range between ≈0.2 and ≈0.8 GPa [24].

Some conventions have been established to distinguish the thermodynamic history of HDA samples. The unrelaxed state of HDA after PIA is called unannealed HDA (uHDA) following the proposition of Nelmes et al. [25]. When uHDA is heated at  $0.1 \leq p \leq 0.5$  GPa its density decreases slightly, and the resulting HDA is called expanded HDA (eHDA) [25]. Another path to eHDA is to decompress very-high-density amorphous ice (VHDA [26]) at 140 K to pressures below 0.4 GPa [27,28]. The exceptional property of eHDA is its high stability with respect to the HDA → LDA transition at ambient pressure. The transition temperature is about 20 K higher

\* Corresponding author.

E-mail address: [thomas.loerting@uibk.ac.at](mailto:thomas.loerting@uibk.ac.at) (T. Loerting).

<sup>1</sup> Present address: Department of Physics, Sapienza—University of Rome, Piazzale Aldo Moro 2, I-00185 Roma, Italy

than for uHDA [13,25,29]. Furthermore, it was proposed to call the HDAs annealed at  $0.3 \leq p_{\text{ann}} \leq 0.8 \text{ GPa}$  relaxed HDA (rHDA) [30]. rHDA is the more general term in the sense that it comprises both denser and expanded HDA states, whereas eHDA represents the subgroup of rHDA states that are expanded with respect to uHDA. In other words, rHDA and eHDA can be used synonymously only at low pressures, at which annealing results in expansion. Suzuki and Tominaga show that uHDA densifies upon annealing above  $p = 0.35 \text{ GPa}$ , i.e., the term eHDA is only appropriate for uHDA samples annealed below  $p = 0.35 \text{ GPa}$  [11].

One of our recent studies [13] is concerned with the relaxation behaviour of uHDA at 0.1 and 0.2 GPa. In this study we have deduced an estimate for the glass transition temperature  $T_g$  of HDA at 0.1 and 0.2 GPa. The procedures leading to these results were commented by Johari [31]. We here reply to the main issues raised by Johari, explain the data published in Ref. [13] in more detail and present related unpublished results, most notably crystallization times.

## 2. Response to Johari's comment

In his comment [31] on our work [13] Johari raises 4 main points, which we discuss here item by item.

(i) *An amorphous solid annealed at a high pressure, quenched to 77 K and recovered at ambient pressure at 77 K has a kinetically arrested configuration of its state at the high pressure. This adds to the instability of the recovered sample with the consequence that the ambient pressure DSC heating scan would contain additional thermal effects (Ref. [31], p. 80).*

This issue has already been addressed partly in our recent response [32] to Johari's criticism [33] on another work by us related to two distinct glass transitions of water at ambient pressure [14]. We agree we study a quench-arrested state and the annealing procedure at high-pressure conditions adds to the thermal effects observed at 1 bar in differential scanning calorimetry (DSC) experiments. In fact, this is exactly the effect we exploit to assess the degree of relaxation in the high-pressure state. However, this effect is not an increase, but a decrease of instability, since we observe an increasing transition temperature  $HDA \rightarrow LDA$   $T_e^{H \rightarrow L}$  with increasing annealing temperature  $T_{\text{ann}}$  and/or annealing time  $t_{\text{ann}}$ . In other words, the thermal stability against transformation to LDA at ambient pressure increases if the high-pressure state is less and less strained, i.e., closer to metastable equilibrium. The effect is illustrated in Fig. 1(a), in which we schematically compare the enthalpy of the highly strained uHDA state, the least strained eHDA state and a state of intermediate strain. LDA is the most stable amorphous state at ambient pressure, by contrast to the situation at high-pressure, e.g., 0.2 GPa. Therefore, HDA will inevitably transform to LDA at ambient pressure, whereas it does not transform to LDA at 0.2 GPa. The transformation temperature depends on the depth of the HDA potential well, see Fig. 1(a). The deeper it is the more thermal energy is required to overcome the barrier. Accordingly, the transformation temperature for eHDA  $\rightarrow$  LDA is higher than for uHDA  $\rightarrow$  LDA. This is clearly seen in our DSC data in Fig. 1(b). The first exotherm caused by the HDA  $\rightarrow$  LDA transition shifts by about 20 K when comparing uHDA and eHDA. Furthermore, we note that the transformations under pressure are less complex than sketched by Johari. Fig. 2 shows the volumetric changes upon compression, which do not involve multiple steps, but just a single step, as discussed in detail below.

(ii) *The  $\alpha$ -relaxation time and  $T_g$  of uHDA determined by using  $T_e$  of the HDA  $\rightarrow$  LDA exotherm seems inconsistent with the precepts of glass relaxation, because  $T_e$  of a DSC exotherm is not proportional to the enthalpy loss. Even if one insists that may be approximately proportional to the area of the exotherm, fitting of a kinetic equation*

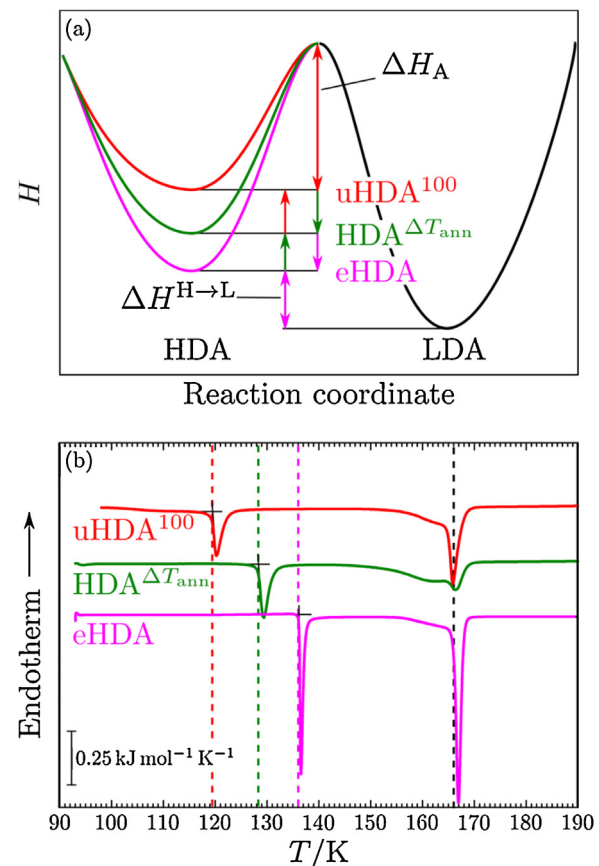


**Fig. 1.** (a) Schematic picture of the molar enthalpy as a function of reaction coordinate for the HDA  $\rightarrow$  LDA transition. Relaxation ( $T_{\text{ann}}$ ) reduces the (molar) enthalpy  $H$  of HDA, therefore  $\Delta H^{H \rightarrow L}$  decreases and  $\Delta H_A$  increases. The lowest  $\Delta H^{H \rightarrow L}$  and the highest  $\Delta H_A$  is seen for eHDA. (b) DSC measurements of differently relaxed HDA samples: uHDA<sup>100</sup> (red), uHDA<sup>100</sup> heated to 130 K at 0.1 GPa with 3 K min<sup>-1</sup> (HDA<sup>ΔT<sub>ann</sub></sup>, green) and eHDA prepared by decompression of VHDA at 140 K to 0.1 GPa (magenta) [29]. The dashed colored lines indicate the onset temperatures of the HDA  $\rightarrow$  LDA transition, and the dashed black line at 166 K helps to recognize the constant temperature of the LDA  $\rightarrow$  I<sub>c</sub> transition (second exotherm). The DSC measurement of the eHDA sample was measured using the Perkin-Elmer DSC 8000, all others the PerkinElmer DSC-4. (For interpretation of the references to color in this figure legend, the reader is referred to the web version of this article.)

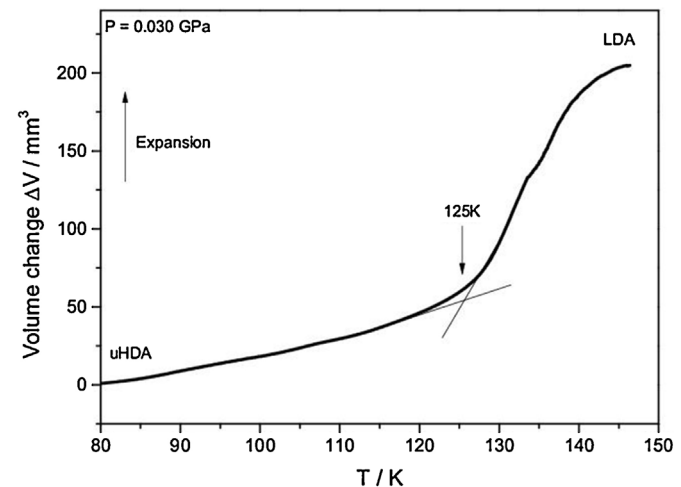


**Fig. 2.** Volume change incurred upon heating 1000 mg of uHDA<sup>77</sup> at initially 0.030 GPa. Once the transformation to LDA commences near 124 K, the pressure is temporarily increased because of the 25% volume expansion, and then returns to 0.03 GPa once the transformation is complete [65]. Note the absence of step-like expansion at 80–120 K. Tangents are drawn to define the onset temperature for the HDA  $\rightarrow$  LDA transition.

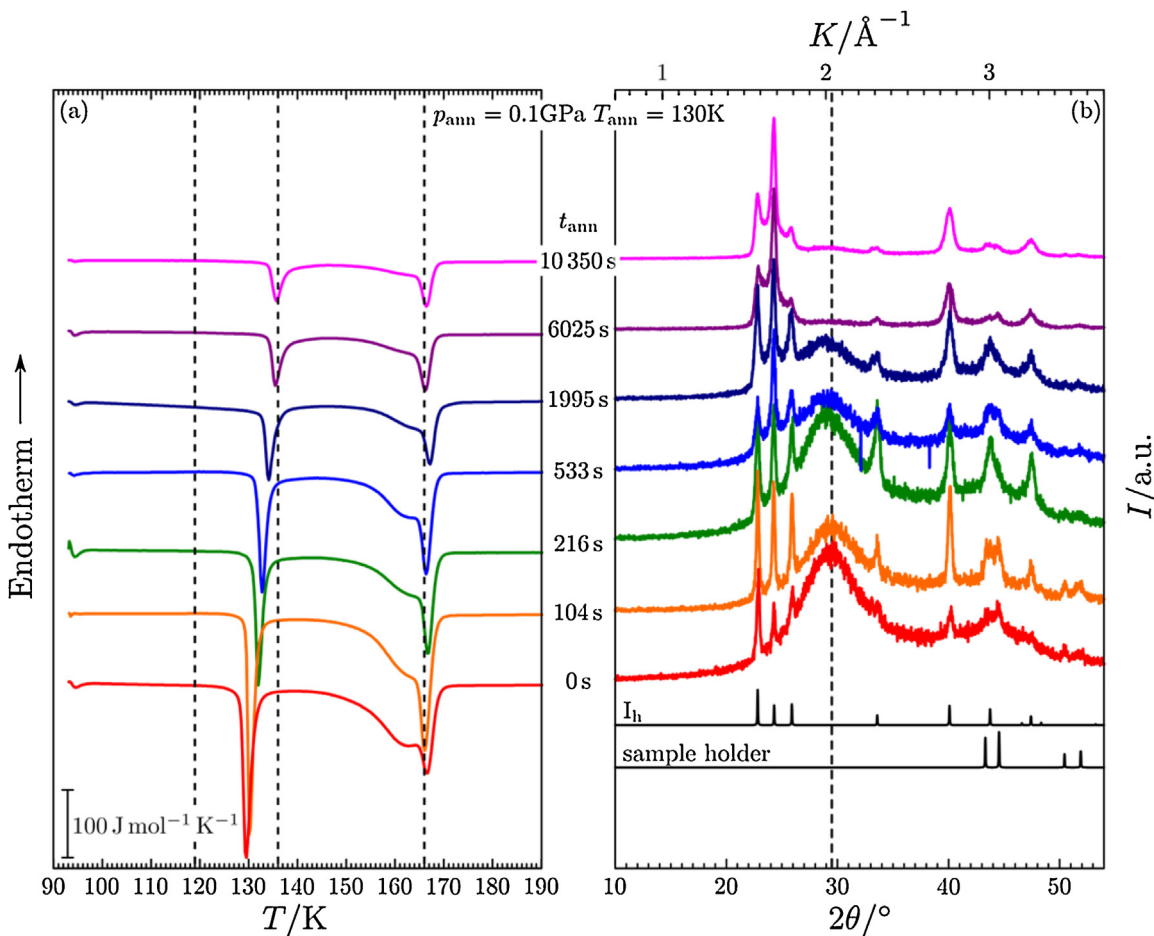


**Fig. 3.** Influence of the annealing time on (a) DSC and (b) XRD measurements of uHDA<sup>100</sup> samples annealed at 0.1 GPa and 130 K. The dashed lines at 119, 136 and 166 K indicate the onset of uHDA<sup>100</sup> → LDA, eHDA → LDA and LDA → I<sub>c</sub>, respectively. The dashed line at 29.5° (2.08 Å) indicates the position of the halo peak of uHDA<sup>100</sup>. The diffractograms are normalized to same maximum intensity. (b, bottom): Theoretical diffractograms of hexagonal ice (I<sub>h</sub>) and the sample holder (Ni-plated Cu) using PowderCell (Version 2.4; BAM, Deutsche Bundesanstalt für Materialforschung und -prüfung). Structural data were taken from Refs. [66–68] for I<sub>h</sub> and from Ref. [69] for Ni and Cu.

would yield the rate constant and not the  $\alpha$ -relaxation time (Ref. [31], p. 80).

As will be discussed in the beginning of Section 4, it would be desirable to use the decrease in the HDA → LDA transition enthalpy as a measure for the degree of relaxation of the sample at high pressure conditions (see Fig. 1(a)). However, this approach has been rendered impracticable because at high pressure slow crystallization of uHDA takes place in addition to its relaxation. As a result, the sample is partially crystalline and partially amorphous after keeping it for a couple of hours, e.g., at 130 K and 0.1 GPa. That is, the HDA → LDA transition enthalpy decreases not only because HDA relaxes, but also because HDA crystallizes. If we knew the exact fraction of crystalline material we could analyze the latent heat on the basis of Joule per mole of amorphous sample. We know the fraction of crystallinity in the sample from our X-ray analysis only to an accuracy of about  $\pm 10\%$ . Because of this rather large uncertainty we do not use latent heat for the analysis of HDA relaxation. In principle, the latent heat associated with the LDA → I<sub>c</sub> transition can be used to assess the fraction of crystalline material too. We emphasize that cubic ice has so far never been prepared as a pure single crystal. When crystallizing from LDA it is not purely cubic but contains some hexagonal stacking faults. There is a current debate on how to name this stacking-disordered form of ice, e.g., as ice I<sub>sd</sub> [34] or as ice I<sub>ch</sub> [35]. Sample parts which have already crystallized at high-pressure conditions do not contribute to this transition, whereas the amorphous fraction (initially HDA) contributes. From this analysis we obtain the crystalline fraction with a

reproducibility of about  $\pm 5\%$  (cf. Section 4.3 here). Also this result is not good enough to make a reliable analysis based on the latent heat for the HDA → LDA transition and, accordingly, not good enough to assess the state of relaxation. The negative values for the fraction of crystalline material seen in chapter 4.3 are a testimony of the uncertainty of such an analysis.

In order to judge on the degree of relaxation of the high-pressure sample, we, therefore, use the onset temperature  $T_e^{\text{H} \rightarrow \text{L}}$  for the HDA → LDA transition exotherm.  $T_e^{\text{H} \rightarrow \text{L}}$  depends on the degree of relaxation of the amorphous fraction of the sample, see Fig. 1. Thus, it can be used to assess the relaxation time in the amorphous HDA matrix at high-pressure conditions. One could argue that the increasing fraction of crystalline domains could result in an additional contribution to the shift of  $T_e^{\text{H} \rightarrow \text{L}}$ . However, in the past an influence of crystallinity on the transition temperature of this transition was not detected [4]. Therefore, we use  $T_e^{\text{H} \rightarrow \text{L}}$  as a measure for the degree of relaxation of the HDA sample at high pressure. Johari is right that we extract rate constants of a relaxation process in uHDA as the result from this procedure. Our observations, e.g., the shift of the halo maximum in the x-ray data shown in Fig. 3(b), indicate these rate constants to be associated with structural relaxations. We then make the connection between the structural relaxation time  $\tau_R$  and the  $\alpha$ -relaxation time  $\tau_\alpha$  of the amorphous matrix. Strictly speaking, there is a difference between  $\tau_R$  and  $\tau_\alpha$ . However, in the present case we argue that this difference is smaller than the uncertainty of our method, so that it is justified to use  $\tau_R$  and  $\tau_\alpha$  interchangeably, i.e.,  $\tau_R \approx \tau_\alpha$ .

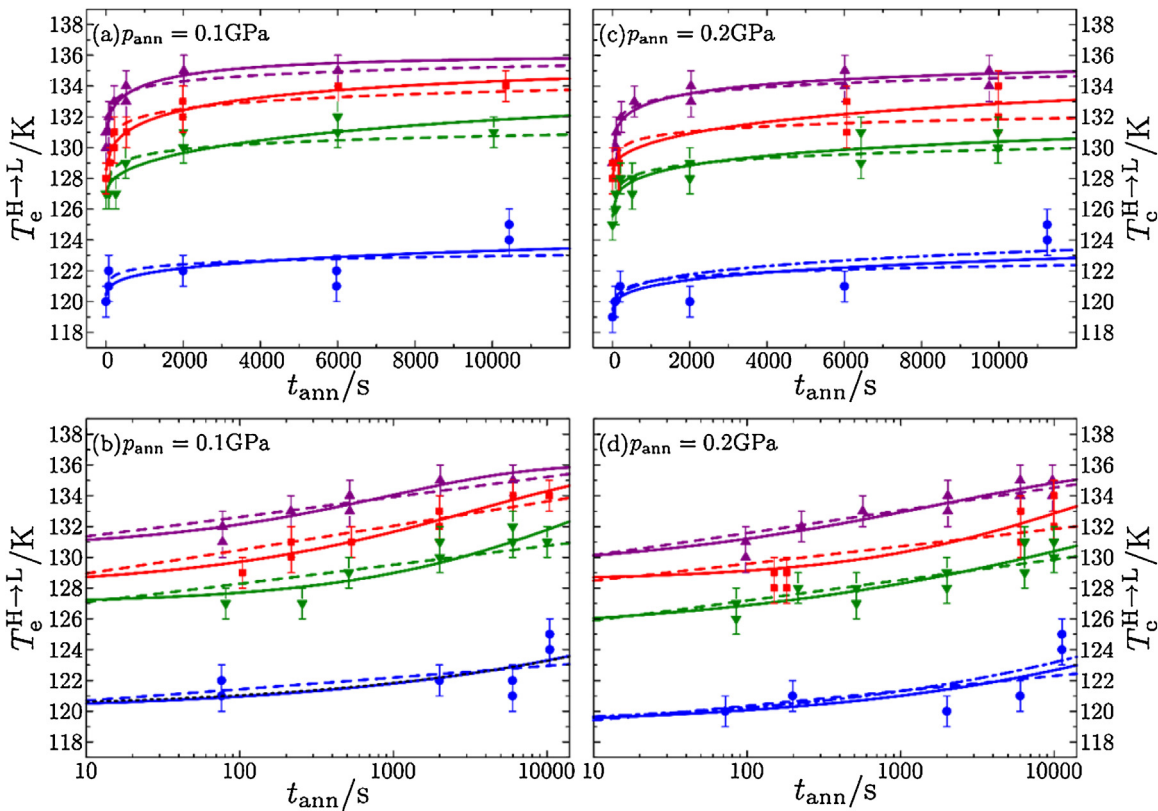


**Fig. 4.** DSC onset temperatures  $T_e^{H \rightarrow L}$  after annealing of uHDA<sup>100</sup> at 0.1 GPa or 0.2 GPa and 110 K (●), 125 K (▼), 130 K (■) or 135 K (▲). Dashed and solid lines show fits with Eqs. (2) and (6), respectively. For the dash-dotted lines  $n$  was fixed (cf. Table 2). Lin-lin (a and c) and lin-log representations are shown (b and d).

This is because the energy landscape describing the HDA megabasin is considered to be rugged [24,36], where the size of the corrugations is small, on the order of 100 K thermal energy, i.e.,  $100 \text{ K} * R \approx 831 \text{ J mol}^{-1}$ . That is, uHDA is arrested in a corrugation at  $T < 100 \text{ K}$ , but appreciably relaxes at  $T > 100 \text{ K}$ . Based on the latent heats observed for the eHDA  $\rightarrow$  LDA and uHDA  $\rightarrow$  LDA transition, the strain levels within the uHDA matrix are comparably small. They are on the order of  $200\text{--}300 \text{ J mol}^{-1}$  as compared to the relaxed state eHDA, i.e., smaller than the size of the corrugations [37]. The strain levels, which would be induced in HDA by an external electric or mechanical field are much larger, and so uHDA is comparably close to equilibrium. Hence, the small additional strain levels in uHDA do not significantly accelerate the relaxation process, and so we regard the difference between  $\tau_R$  and  $\tau_\alpha$  to be insignificant. Most notably, this difference is much smaller than the uncertainty of typically 20–50% associated with extracting  $\tau_R$  by fitting the data in Fig. 4 (see Tables 1 and 2 for 125–135 K). Furthermore, we obviously regard the amorphous matrix to be glassy, converting to the ultraviscous liquid HDL above  $T_g$ . We appreciate there is a literature debate [38–40] on this issue. Only in case one does not regard the amorphous ice to be glassy then  $\alpha$ -relaxation would not be an appropriate terminology.

(iii) *The pressure at  $T_{ann}$  of uHDA is higher than the pressure at which  $T_e$  was determined to obtain  $\tau$ . This does not fulfill the requirements of the Arrhenius equation, namely, that  $\tau$  and  $T$  be measured at the same pressure. Therefore, the slope of their  $\ln(\tau)$  against  $1/T_{ann}$  plot is not meaningful, and the significance of activation energy of 34 kJ mol<sup>-1</sup> at 0.1 GPa and 40 kJ mol<sup>-1</sup> at 0.2 GPa determined from such plots becomes questionable (Ref. [31], p. 80).*

Indeed, the pressure at which uHDA was annealed (0.1 GPa or 0.2 GPa) is higher than the pressure at which the onset of the HDA  $\rightarrow$  LDA transition temperature  $T_e^{H \rightarrow L}$  was measured (1 bar). However, as discussed above, the sample was quench-arrested and

so the property measured at ambient pressure by DSC is related to the structural state after annealing at  $T_{ann}$  and  $p_{ann}$  for  $t_{ann}$ . Hence, application of the Arrhenius analysis is justified, providing the activation energy of uHDA relaxation at high-pressure conditions. No thermal effects are known to be introduced during quenching, recovery (decompression) and the procedure of pushing out the sample of the high-pressure cylinder. Even if there were thermal effects, they would be the same for all samples of a certain dataset (same  $T_{ann}$  and  $p_{ann}$ ) and basically also the same for the samples at different  $p_{ann}$ , thus still allowing for an Arrhenius analysis.

(iv) *It is operationally meaningless to speak of  $T_g$  of a strained state of an amorphous solid, because the strain is permanently lost on heating. uHDA does not have a  $T_g$ , and is not formed by cooling ultraviscous water (Ref. [31], p. 80).*

In contrast to Johari's view there are studies, which relate uHDA with a liquid state. Klotz et al. found a similarity between uHDA's structure at 0.7 GPa and the structure of liquid water at 0.4 GPa [7]. Klotz et al. [8] and Salzmann et al. [30] demonstrated that uHDA under pressure crystallizes into the same polymorphs as liquid water under pressure. This again implies a structural similarity of uHDA and the liquid. Johari is correct in stating uHDA is not formed by cooling ultraviscous water at ambient pressure. In fact, we have recently shown that ultraviscous, high-density liquid water (HDL) transforms to eHDA upon cooling at ambient pressure, whereas ultraviscous, low-density liquid water (LDL) transforms to LDA [14]. Mishima and Suzuki demonstrated it is possible to vitrify emulsified water at  $\approx 0.5 \text{ GPa}$  using cooling rates of  $10^3\text{--}10^4 \text{ K/s}$  [6]. They conclude what they obtain after vitrification is HDA, even though it cannot be judged from the x-ray photographs whether it resembles eHDA or uHDA.

Johari's statement "uHDA does not have a  $T_g$ " is based on a schematic illustration of enthalpy and volume (Fig. 1 in Ref. [31]).

**Table 1**

Relaxation kinetics parameters obtained from fitting data at 0.1 GPa in Fig. 4(a) with Eq. (6) (Fit-Variant ‘‘R-Fix’’ using a fixed value for  $T_{e,0}^{H \rightarrow L}$ ), Eq. (6) (Fit-Variant ‘‘R’’ using  $T_{e,0}^{H \rightarrow L}$  as a fitting parameter) and Eq. (2) (Fit-Variant ‘‘Log’’).  $\chi^2$ ,  $R^2$  and SSE are statistic measures.

$T_{\text{ann}}/\text{K}$	Fit-Variant	Restrictions	$\chi^2$	$R^2$	SSE	$T_{e,0}^{H \rightarrow L}/\text{K}$	$B/\text{K}$	$\tau_R/\text{s}$	$n$
110	R-Fix	–	1.1103	0.5636	8.882	*120.0	–	$1.7 \times 10^6 \pm 5.6 \times 10^6$	$0.286 \pm 0.162$
	R	$n \leq 0.286$	1.2604	0.5046	8.823	$120.1 \pm 0.8$	–	$2.0 \times 10^6 \pm 8.3 \times 10^6$	$0.286 \pm 0.221$
	Log	–	1.2382	0.5134	9.906	$119.9 \pm 0.7$	$0.76 \pm 0.24$	$\dagger 2.1 \times 10^{13} \pm 2.0 \times 10^{14}$	–
125	R-Fix	–	0.6552	0.8296	7.863	*127.0	–	$1.77 \times 10^4 \pm 6.5 \times 10^3$	$0.485 \pm 0.099$
	R	–	0.6702	0.8258	7.372	$126.6 \pm 0.6$	–	$1.66 \times 10^4 \pm 6.1 \times 10^3$	$0.434 \pm 0.114$
	Log	–	1.3309	0.6540	15.971	$125.8 \pm 0.7$	$1.24 \pm 0.24$	$\dagger 1.6 \times 10^5 \pm 4.1 \times 10^5$	–
130	R-Fix	–	0.1866	0.9634	2.052	*128.0	–	$3.40 \times 10^3 \pm 4.7 \times 10^2$	$0.404 \pm 0.038$
	R	$n \leq 0.5$	0.2044	0.9600	2.043	$127.9 \pm 0.3$	–	$3.32 \times 10^3 \pm 6.1 \times 10^2$	$0.400 \pm 0.046$
	Log	–	0.6135	0.8798	6.748	$127.3 \pm 0.5$	$1.58 \pm 0.17$	$\dagger 3.0 \times 10^3 \pm 2.6 \times 10^3$	–
135	R-Fix	–	0.2848	0.9103	2.848	*130.5	–	$9.2 \times 10^2 \pm 2.1 \times 10^2$	$0.467 \pm 0.080$
	R	–	0.3139	0.9011	2.826	$130.4 \pm 0.4$	–	$8.8 \times 10^2 \pm 2.7 \times 10^2$	$0.457 \pm 0.091$
	Log	–	0.4827	0.8479	4.827	$130.0 \pm 0.4$	$0.00 \pm 0.17$	$\dagger 7.7 \times 10^2 \pm 7.5 \times 10^2$	–

\*Values have been fixed at the mean value of all data obtained for 0 s annealing time for the respective  $T_{\text{ann}}$  and  $p_{\text{ann}}$ . †Values are not obtained by a fit, but calculated from Eq. 4 using the relevant parameters.

**Table 2**

Relaxation kinetics parameters obtained from fitting data at 0.2 GPa in Fig. 4(c) with Eq. (6) (Fit-Variant ‘‘R-Fix’’ using a fixed value for  $T_{e,0}^{H \rightarrow L}$ ), Eq. (6) (Fit-Variant ‘‘R’’ using  $T_{e,0}^{H \rightarrow L}$  as a fitting parameter) and Eq. (2) (Fit-Variant ‘‘Log’’).  $\chi^2$ ,  $R^2$  and SSE are statistic measures.

$T_{\text{ann}}/\text{K}$	Fit-Variant	Restrictions	$\chi^2$	$R^2$	SSE	$T_{e,0}^{H \rightarrow L}/\text{K}$	$B/\text{K}$	$\tau_R/\text{s}$	$n$
110	R-Fix	$n \leq 0.286$	1.6022	0.5132	14.420	*1190	–	$1.4 \times 10^6 \pm 4.0 \times 10^6$	$0.286 \pm 0.137$
	R-Fix	$n = 0.286$	1.4419	0.5619	14.419	*119.0	–	$1.4 \times 10^6 \pm 8.2 \times 10^5$	0.286
	R	$n \leq 0.286$	2.0037	0.3911	16.030	$119.0 \pm 1.4$	–	$8.4 \times 10^5 \pm 2.5 \times 10^6$	$0.286 \pm 0.207$
	Log	–	2.0046	0.3909	18.041	$118.4 \pm 1.1$	$0.97 \pm 0.36$	$\dagger 2.6 \times 10^{11} \pm 2.5 \times 10^{12}$	–
125	R-Fix	–	0.4419	0.8711	5.744	*125.0	–	$4.2 \times 10^4 \pm 2.1 \times 10^4$	$0.278 \pm 0.044$
	R	–	0.4786	0.8604	5.743	$125.0 \pm 0.5$	–	$4.2 \times 10^4 \pm 2.2 \times 10^4$	$0.279 \pm 0.057$
	Log	–	0.5993	0.8252	7.791	$124.5 \pm 0.5$	$1.34 \pm 0.16$	$\dagger 2.6 \times 10^5 \pm 4.2 \times 10^5$	–
130	R-Fix	–	1.0166	0.7962	8.133	*128.5	–	$1.32 \times 10^4 \pm 6.1 \times 10^3$	$0.500 \pm 0.177$
	R	–	0.9767	0.8042	6.837	$128.1 \pm 0.7$	–	$1.18 \times 10^4 \pm 4.9 \times 10^3$	$0.500 \pm 0.223$
	Log	–	2.2960	0.5398	18.368	$127.3 \pm 0.9$	$1.14 \pm 0.33$	$\dagger 6.7 \times 10^4 \pm 2.4 \times 10^5$	–
135	R-Fix	–	0.3247	0.9210	3.896	*129.0	–	$1.79 \times 10^3 \pm 4.0 \times 10^2$	$0.337 \pm 0.048$
	R	–	0.3527	0.9142	3.879	$128.9 \pm 0.4$	–	$1.71 \times 10^3 \pm 5.3 \times 10^2$	$0.333 \pm 0.055$
	Log	–	0.4126	0.8996	4.951	$128.6 \pm 0.4$	$1.48 \pm 0.14$	$\dagger 1.5 \times 10^3 \pm 1.1 \times 10^3$	–

\*Values have been fixed at the mean value of all data obtained for 0 s annealing time for the respective  $T_{\text{ann}}$  and  $p_{\text{ann}}$ . †Values are not obtained by a fit, but calculated from Eq. 4 using the relevant parameters.

The transition sequence transforming uHDA to LDA at ambient pressure shown in his schematic illustration involves two step-like conversions, uHDA → eHDA (onset at 92 K) and eHDA → LDA (onset at 114 K). Johari’s schematic illustration is falsified by experiment. Fig. 2 here shows experimentally measured volume change data observed upon heating uHDA at low pressures. Most notably, there is only a single step-like conversion, uHDA → LDA (onset at 125 K at 0.03 GPa). The step-like change in volume indicating uHDA → eHDA suggested by Johari is not observed in our experiment. Also others, e.g., Mishima et al. [41], have never reported on the uHDA → eHDA transition at ambient pressure, even though they were following volume changes and thermal effects upon heating uHDA. The Tian-Calvet calorimetry data quoted by Johari to indicate a step-like transition was interpreted by Handa et al. as ‘‘slow enthalpy relaxation’’, not as a step-like transition [42]. In other words, the relaxation process leading from uHDA to eHDA is so slow at 1 bar that eHDA cannot be accessed by annealing uHDA at 1 bar. Our understanding of the processes taking place upon heating uHDA at 1 bar is as follows: uHDA represents a strained state of HDA slowly relaxing towards the metastable equilibrium, i.e., to eHDA. However, the eHDA state cannot be reached at 1 bar (or slightly elevated pressure) and <120 K because the relaxation times are far beyond time scales accessible in laboratory experiments. The time required to convert uHDA to LDA, by contrast, is much shorter. For this reason uHDA transforms to LDA at 1 bar long before the expanded and metastably equilibrated state eHDA can

be reached. In order to be able to reach the eHDA state it is necessary to suppress transformation to LDA. This is typically done by applying external pressure of 0.1 GPa or more. Such pressures were applied in the first study reporting the expanded HDA state by Nelmes et al. [25]. We have followed a similar strategy here and in our previous study reporting the relaxation times of uHDA [13]. In other words, uHDA can be brought to the metastable equilibrium by annealing at 0.1 GPa or 0.2 GPa, but not by annealing at 1 bar. This metastable equilibrium phase is called eHDA (if relaxation times are 100 s or more) or high-density liquid water HDL (if relaxation times are less than 100 s). We note the annealing times of up to 10 ks used in our study are not sufficient to reach the fully equilibrated state—however, the sample is brought close to the equilibrated state, with the caveat that a certain fraction of the sample crystallizes.

In short, HDL has a  $T_g$  thermodynamically connecting it with eHDA. eHDA in turn can be accessed from uHDA by relaxation of strain, provided the time scale of relaxation is shorter than the time scale of conversion to LDA. This is the case at elevated pressure, e.g., 0.1 GPa, but not at ambient pressure. Consequently, there is only one glass transition thermodynamically connecting HDA and HDL, but not two distinct glass transitions, one pertaining to eHDA and one pertaining to uHDA. Thus, the experiments reported here are aimed at obtaining quantitative information about  $T_g(\text{HDA})$  based on monitoring the relaxation taking place within uHDA at 0.1 and 0.2 GPa.

Having clarified these issues, we now move on to show the data and data analysis reported in our earlier work [13] in the following sections in more detail.

### 3. Experimental details

#### 3.1. Preparation of uHDA

For sample preparation 700  $\mu\text{l}$  of pure water were pipetted in a precooled indium container at 77 K. Water freezes to hexagonal ice I<sub>h</sub>, and the container including the sample was inserted in a high-pressure cell of 10 mm diameter. This procedure was first used by Mishima et al. [5], and has the advantage that indium eliminates friction between the ice sample and the high-pressure cell. The cell was then placed in a material testing machine (Zwick model BZ100/TL3S) and the sample was precompressed at 77 K to 0.9 GPa. This procedure removes air trapped between single ice crystals and produces a compact, bubble-free ice cylinder. Subsequently the sample is decompressed to 0.01 GPa. By not decompressing to ambient pressure formation of (micro)cracks in the ice cylinder is avoided [24]. The compression and decompression rate were 0.09 GPa min<sup>-1</sup>. Thereafter the sample was heated to 100 K at an arbitrary rate. At 100 K the sample was compressed to 1.4 GPa, resulting in transformation of ice I<sub>h</sub> to uHDA<sup>100</sup>.<sup>1</sup> Please note, the original protocol employed by Mishima et al. involves compression at 77 K rather than at 100 K [5]. The uHDA produced at 77 K is even more strained than the uHDA<sup>100</sup> produced here. This can be appreciated by comparing the onset temperatures for the thermally induced HDA  $\rightarrow$  LDA transition  $T_e^{\text{H} \rightarrow \text{L}}$ . In our experiments  $T_e^{\text{H} \rightarrow \text{L}}$  shifts from 116 K (see Fig. 1(b) in Ref. [13]) to 118 K (see Fig. 1(b) here) when amorphizing at 100 K instead of 77 K.

#### 3.2. Annealing at 0.1 GPa or 0.2 GPa

The pressure was then released at 100 K from 1.4 GPa to either 0.1 or 0.2 GPa, which are the annealing pressures  $p_{\text{ann}}$ . The rates of compression and decompression were 0.06 GPa min<sup>-1</sup>. The samples were then heated isobarically at  $p_{\text{ann}}$  with a rate of 3 K min<sup>-1</sup> to either 110, 125, 130 or 135 K, the annealing temperatures  $T_{\text{ann}}$ . When the desired  $T_{\text{ann}}$  was reached, samples were kept at isobaric-isothermal conditions for annealing times  $t_{\text{ann}}$  of up to 3 h. After  $t_{\text{ann}}$  had passed the samples were quenched with liquid nitrogen to 77 K, while retaining the sample pressurized. The pressure was then released with 0.06 or 0.13 GPa min<sup>-1</sup> and the samples were pushed out of the high-pressure cell and stored at 77 K and 1 bar. We paid attention that the pressure during the pushing out procedure did not exceed 0.25 GPa.

#### 3.3. Ex situ analysis using DSC and XRD

In order to investigate the effect of annealing for  $t_{\text{ann}}$  at  $T_{\text{ann}}$  and  $p_{\text{ann}}$  we characterized the quench-recovered samples *ex situ* by differential scanning calorimetry (DSC) and x-ray diffraction (XRD), both at (sub)ambient pressure. For the DSC measurements we used a PerkinElmer DSC-4. Small chips of the sample ( $\approx 1$ –30 mg) were placed in screwable steel crucibles at 77 K, which in turn were placed in the precooled DSC at 93 K. Then 3 heating scans were performed on each sample at a heating rate of 10 K min<sup>-1</sup> in all cases. Two scans from 93 to 253 K and one scan from 253 to 293 K. The first scan shows the polyamorphic transition HDA  $\rightarrow$  LDA, the crystallization LDA  $\rightarrow$  ice I<sub>c</sub> and the broad polytypic transition ice

<sup>1</sup> The superscript 100 indicates the temperature of pressure-induced amorphization to be 100 K.

I<sub>c</sub>  $\rightarrow$  ice I<sub>h</sub>. Whereas the former two transitions are easily identified in Fig. 1(b), the latter releases not enough latent heat to be visible at the level of magnification used for Fig. 1(b). All three transitions are exothermic and cannot be reversed by cooling at 1 bar. Therefore, the second heating scan shows no transition and serves as base line. The third scan shows the massive endotherm due to melting of hexagonal ice I<sub>h</sub>. From this peak the sample mass is extracted via the known melting enthalpy of water (6.012 kJ mol<sup>-1</sup> [43]). All traces shown in Fig. 1(b) represent baseline corrected thermograms, i.e., scan 1 minus scan 2. The heat capacity  $c_p$  is calculated subsequently using the heating rate and the sample mass as obtained from scan 3. X-ray diffractograms were recorded after breaking small chip from the sample, powdering them and cold-loading the powder at  $\approx 80$  K onto a nickel-plated copper sample holder in flat geometry. The low-temperature chamber by Anton-Paar holding the sample holder is then pumped to approximately 10<sup>-2</sup> mbar. A Siemens D 5000 diffractometer equipped with a Cu-K $\alpha$  x-ray source ( $\lambda = 1.541 \text{ \AA}$ ) is used to record diffractograms from  $2\theta = 10^\circ$  ( $d = 0.71 \text{ \AA}$ ) to  $2\theta = 54^\circ$  ( $d = 3.70 \text{ \AA}$ ) using a step width of 0.02° and acquisition times of 1 s at each step. DSC characterization was done on all samples, XRD measurements were done for all samples annealed at 125, 130 and 135 K (both at 0.1 and 0.2 GPa). From the samples annealed at 110 K XRD measurements were taken only for the shortest (0 s) and longest ( $\approx 10$  ks) annealing time  $t_{\text{ann}}$ .

### 4. Results & discussion

#### 4.1. Qualitative features of thermograms and diffractograms

The main part of our quantitative analysis presented hereafter is based on the thermograms. Diffractograms are used for assessing the samples qualitatively. The first feature of the DSC measurements we discuss is the onset temperature of the HDA  $\rightarrow$  LDA transition—denoted  $T_e^{\text{H} \rightarrow \text{L}}$  (see Ref. [44] for definition). The influence of the thermodynamic history on the first exotherm is apparent in Fig. 1(b).  $T_e^{\text{H} \rightarrow \text{L}}$  is influenced by the annealing temperature  $T_{\text{ann}}$  as well as the annealing time  $t_{\text{ann}}$  such that higher  $T_{\text{ann}}$  and longer  $t_{\text{ann}}$  result in an upshift of  $T_e^{\text{H} \rightarrow \text{L}}$ . By contrast, the second exotherm, indicating crystallization of LDA to cubic ice I<sub>c</sub> is not shifting to higher temperatures, i.e., it does not depend on the annealing procedure. This is evident from the peak temperature  $T_p^{\text{L} \rightarrow \text{I}_c}$  ( $\approx 166$ –167 K) (see Ref. [44] for definition). In this case we use the peak temperature  $T_p^{\text{L} \rightarrow \text{I}_c}$  rather than the onset temperature  $T_e^{\text{L} \rightarrow \text{I}_c}$ , since the shape of the LDA  $\rightarrow$  I<sub>c</sub> transition changes somewhat with thermal history, impeding a unique determination of  $T_e^{\text{L} \rightarrow \text{I}_c}$ . Now let us discuss one data set in detail. In Fig. 3(a) DSC scans of uHDA<sup>100</sup> samples are shown after annealing at  $p_{\text{ann}} = 0.1$  GPa and  $T_{\text{ann}} = 130$  K for the given  $t_{\text{ann}}$ . Upon increasing  $t_{\text{ann}}$  not only  $T_e^{\text{H} \rightarrow \text{L}}$  is increased, but also the area of both exotherms decreases, that is the enthalpy of the HDA  $\rightarrow$  LDA transition  $\Delta H^{\text{H} \rightarrow \text{L}}$  in case of the first exotherm and the enthalpy of the LDA  $\rightarrow$  I<sub>c</sub> transition  $\Delta H^{\text{L} \rightarrow \text{I}_c}$  in case of the second exotherm. One reason for the significant decrease in these transition enthalpies is partial crystallization of the samples during the annealing procedure. Gradual crystallization of uHDA in the pressure range studied here has already been reported by Salzmann et al. [45] and Seidl et al. [46,47]. Gradual crystallization with increasing  $t_{\text{ann}}$  is also observed here as evidenced from the increasing intensity of Bragg peaks in the XRD measurements depicted in Fig. 3(b). The increase of the crystalline fraction is very slow at low  $T_{\text{ann}}$ , but becomes faster at higher  $T_{\text{ann}}$ . As mentioned above the crystalline fraction directly affects the observed latent heats  $\Delta H^{\text{H} \rightarrow \text{L}}$ , impairing our ability of judging on the state of relaxation based on latent heats. Instead we use  $T_e^{\text{H} \rightarrow \text{L}}$  as a measure for relaxation in the amorphous fraction of the sample. The rationale behind this approach is explained using the

**Table 3**

Arrhenius-parameters obtained from fitting the temperature dependence of the relaxation times  $\tau_R(T)$  (from Tables 1 and 2) for 0.1 and 0.2 GPa with Eq. (7).  $\chi^2$ ,  $R^2$  and SSE are statistic measures.

Fit-Variant	Restrictions	$\chi^2$	$R^2$	SSE	$\tau_{R,\infty}/\text{s}$	$E_A/\text{kJ mol}^{-1}$
$p_{\text{ann}} = 0.1 \text{ GPa}$						
R-Fix	–	0.1194	0.9878	0.239	$4.2 \times 10^{-13} \pm 8.0 \times 10^{-13}$	$39.6 \pm 2.3$
R	–	0.0485	0.9927	0.097	$1.9 \times 10^{-13} \pm 2.7 \times 10^{-13}$	$40.5 \pm 1.7$
Log	–	0.0720	0.7510	0.144	$1.18 \times 10^{-13} \pm 1.2 \times 10^{-12}$	$40.9 \pm 12.2$
Log	$E_A \geq 80 \text{ kJ mol}^{-1}$	7.1571	-23.7423	14.314	$9.193 \times 10^{-29} \pm 6.3 \times 10^{-27}$	$80.0 \pm 88.7$
$p_{\text{ann}} = 0.2 \text{ GPa}$						
R-Fix	–	1.2713	0.6188	2.543	$2.4 \times 10^{-10} \pm 7.3 \times 10^{-10}$	$33.3 \pm 3.5$
R	–	1.2097	0.5214	2.419	$6.04 \times 10^{-11} \pm 3.4 \times 10^{-10}$	$34.9 \pm 6.7$
Log	–	0.0274	0.8263	0.055	$9.30 \times 10^{-26} \pm 4.1 \times 10^{-25}$	$72.9 \pm 5.7$

schematic drawing in Fig. 1(a). In this drawing uHDA<sup>100</sup> (red) has the highest enthalpy since it is the least relaxed HDA form. Relaxing uHDA<sup>100</sup> leads to a decrease in the enthalpy, HDA becomes more stable (green)—a process progressing with time and progressing faster at higher temperature. The lowest enthalpy state in this picture is eHDA (magenta), because it is the most stable HDA form at ambient pressure known so far. The decrease in HDA's enthalpy due to relaxation leads both to a decrease of  $\Delta H^{H \rightarrow L}$  and an increase of  $T_e^{H \rightarrow L}$ . We here consider the HDA → LDA transition state to be a unique state, which is independent of the initial strain level in HDA. That is, a decrease in the enthalpy of HDA leads in turn to an increase in the molar activation enthalpy  $\Delta H_A$ , such that more thermal energy, i.e., higher  $T_e^{H \rightarrow L}$ , is required to cross the transition state. In other words,  $T_e^{H \rightarrow L}$  obtained from ambient pressure experiments on quench-recovered samples is suitable for assessing the degree of relaxation of the HDA sample at high-pressure conditions.

#### 4.2. Quantitative analysis

All HDA → LDA transition temperatures  $T_e^{H \rightarrow L}$  are collected in Fig. 4. Obviously, there is barely any shift of  $T_e^{H \rightarrow L}$  for the series at  $T_{\text{ann}} = 110 \text{ K}$  (blue symbols and lines), whereas  $T_e^{H \rightarrow L}$  increases within the first 2000 s for higher  $T_{\text{ann}}$ . This means relaxation at  $T_{\text{ann}} = 110 \text{ K}$  is too slow to be significant on the three hours time scale, whereas it is fast enough at higher  $T_{\text{ann}}$ . In order to extract a time constant for the relaxation, which is the relaxation time  $\tau_R$ , based on the shift of  $T_e^{H \rightarrow L}$  two different quantitative approaches are used. First, a fit with a logarithmic function and second a fit with a relaxation function.

##### 4.2.1. Fit with a logarithmic function

The variant to fit the shift in onset temperature  $T_e^{H \rightarrow L}$  as a function of annealing time  $t_{\text{ann}}$  by a logarithmic function is based on the approach of Koza et al. [48]. These authors studied the HDA → LDA transition at ambient pressure based on the shift of the first diffraction maximum in neutron scattering experiments. They found HDA relaxes prior to the transition to LDA and fitted this contribution by a  $\log_e(t)$  term [48]. This study was amongst others based on the work of Karpov and Grimsditch, who described the change of sound velocity in amorphous SiO<sub>2</sub> as a function of time on basis of a double-well potential model with [49]:

$$\Delta v(t) = A + B \log_{10}(t) \quad (1)$$

The analogous function

$$T_e^{H \rightarrow L}(t) = T_{e,0}^{H \rightarrow L} + B \log_{10}(t_{\text{ann}} + 1) \quad (2)$$

was used here to fit  $T_e^{H \rightarrow L}$ . Instead of a  $\log_{10}(t_{\text{ann}})$  dependence a  $\log_{10}(t_{\text{ann}} + 1)$  dependence was used in order to enable the function to also fit the data points at  $t_{\text{ann}} = 0 \text{ s}$ .  $T_{e,0}^{H \rightarrow L}$  is the transition

temperature at  $t = 0 \text{ s}$  and was used as fitting parameter alongside  $B$ . The data sets were fitted using OriginPro 8G. The fits according to Eq. (2) are shown as dashed curves in Fig. 4(a) and (c). These dashed curves are straight lines in the logarithmic plots shown in Fig. 4(b) and (d). All fitting parameters are summarized in Tables 1 and 2 for  $p_{\text{ann}} = 0.1 \text{ GPa}$  and  $p_{\text{ann}} = 0.2 \text{ GPa}$ , respectively.

Since it is of interest to extract relaxation times from the data the following procedure was used here: First, an onset transition temperature  $T_{e,\infty}^{H \rightarrow L} = 136 \text{ K}$  was assumed to be the highest possible value for  $T_e^{H \rightarrow L}$ , i.e., the onset transition temperature of the most relaxed state. This is based on two studies by Winkel et al. resulting in  $T_e^{H \rightarrow L} = 136 \text{ K}$  [27,29]. Also in the present study we find the same value (cf. Fig. 1(b)). Therefore, this value was used. Second, the relaxation time  $\tau_R$  is typically defined as the time after which a fraction of  $(1 - 1/e)$  of the total relaxation is covered. This is described by the relation

$$T_e^{H \rightarrow L}(\tau_R) = T_{e,0}^{H \rightarrow L} + \left(1 - \frac{1}{e}\right)(T_{e,\infty}^{H \rightarrow L} - T_{e,0}^{H \rightarrow L}) \quad (3)$$

In combination with Eq. (2) this yields

$$\tau_R = 10^{\frac{\left(1 - \frac{1}{e}\right)(T_{e,\infty}^{H \rightarrow L} - T_{e,0}^{H \rightarrow L})}{B}} - 1. \quad (4)$$

The relaxation times calculated with this relation are also listed in Tables 1 and 2 together with the errors as calculated using Gaussian error propagation.

##### 4.2.2. Fit with a relaxation function

As a second fit function a classic relaxation function (see, e.g., Ref. [50]) of the form

$$T_e^{H \rightarrow L}(t_{\text{ann}}) = T_{e,\infty}^{H \rightarrow L} + (T_{e,0}^{H \rightarrow L} - T_{e,\infty}^{H \rightarrow L}) e^{-\left(\frac{t_{\text{ann}}}{\tau_R}\right)} \quad (5)$$

was considered, slightly modifying it by introducing the exponent  $n$ , in an analogous way to the Kohlrausch-Williams-Watts-Function (see, e.g., Refs. [36,50,51]):

$$T_e^{H \rightarrow L}(t_{\text{ann}}) = T_{e,\infty}^{H \rightarrow L} + (T_{e,0}^{H \rightarrow L} - T_{e,\infty}^{H \rightarrow L}) e^{-\left(\frac{t_{\text{ann}}}{\tau_R}\right)^n}. \quad (6)$$

Here  $T_{e,0}^{H \rightarrow L}$  denotes the onset transition temperature at  $t_{\text{ann}} = 0 \text{ s}$ ,  $\tau_R$  the relaxation time and  $T_{e,\infty}^{H \rightarrow L}$  denotes again the onset transition temperature of eHDA (136 K). The fits according to Eq. (6) were done using OriginPro 8G. The fitting parameters are  $n$  and  $\tau_R$ , whereas  $T_{e,0}^{H \rightarrow L}$  is fixed at the mean value of the data points at  $t_{\text{ann}} = 0 \text{ s}$  of the respective data set. The resulting fits are shown as solid curves in Fig. 4. All fitting parameters are listed in Tables 1 and 2 for  $p_{\text{ann}} = 0.1 \text{ GPa}$  and  $p_{\text{ann}} = 0.2 \text{ GPa}$ , respectively (Variant: R-Fix). Please note that the parameter  $n$  was sometimes restricted. Furthermore, also fits were performed where  $T_{e,0}^{H \rightarrow L}$  was also used as a fitting parameter. Since the results are almost indistinguishable from the approach with fixed  $T_{e,0}^{H \rightarrow L}$ , they have been omitted for

**Table 4**

Estimated glass transition temperatures  $T_g$  obtained by extrapolation of the fit data in Table 3 to  $\tau_R = 100$  s.

Fit-Variant	Restrictions	$T_g/K$
R-Fix	$p = 0.1 \text{ GPa}$	$144 \pm 1$
R	–	$144 \pm 1$
Log	–	$143 \pm 4$
Log	$E_A \geq 80 \text{ kJ mol}^{-1}$	$139 \pm 6$
R-Fix	$p = 0.2 \text{ GPa}$	$150 \pm 3$
R	–	$149 \pm 5$
Log	–	$141 \pm 1$

clarity in the figures (interested readers are referred to Ref. [52] for more detail). However, all corresponding fitting parameters are listed in Tables 1–4 (Variant: R).

The parameter  $n$  takes values between 0.3 and 0.5, consistently for all data sets. That is, HDA relaxation is sub-monoexponential. Such a stretched exponential relaxation was also found for the ultraslow dynamics in HDA as probed by  $^2\text{H}$  NMR stimulated echoes [53]. In these experiments the parameter  $n$  (called Kohlrausch parameter  $\beta$  there) was found to be between 0.8 and 0.9 [53]. In other words, the ultraslow dynamics probed in NMR experiments for HDA at ambient pressure is closer to mono-exponential relaxation (less stretched) than the slow structural relaxation dynamics at high pressure conditions probed here. It would be of great interest to study the ultraslow relaxation in HDA near its glass transition temperature using NMR also at high pressure conditions.

In contrast to NMR measurements, HDA has been studied under high-pressure and low-temperature conditions near 130 K using dielectric relaxation techniques [54–56]. In these studies the dielectric spectra were found to be best described by the symmetrical Cole–Cole distribution function. Almost independent of pressure up to about 1 GPa the exponent (called distribution factor  $1-\alpha$  there) was found to be between 0.6 and 0.7 [54–56]. For HDA samples measured at ambient pressure using dielectric relaxation spectroscopy the near-to-peak Kohlrausch exponent was found to be 0.5, thus very close to the value that we find here for  $n$  (see Fig. 10(b) in Ref. [40]). By contrast, for ice I<sub>h</sub> and LDA samples the Kohlrausch exponent is much closer to 1.

#### 4.2.3. Comparison between the two fit functions

Significantly different fit parameters (see Table 1) are found for the logarithmic fit as compared to the relaxation function fit. The differences are larger at lower annealing temperatures. The logarithmic fit yields values for the relaxation times that are up to seven orders of magnitude larger than the ones obtained by the relaxation function fit. Further the relative errors of the logarithmic fits are always larger than the corresponding errors of the relaxation function fit. This is not surprising, since also the statistic measures of the fit always qualify the logarithmic fit as the least suitable variant (cf. Tables 1 and 2). That is, we regard the logarithmic fit function results to be clearly inferior to the relaxation function fit, not grasping the underlying physics. In spite of this and for the sake of completeness we include the results of the logarithmic fit procedure in this manuscript.

#### 4.2.4. Estimation of $T_g$

As shown in Fig. 4 we observe a clear relaxation process in uHDA<sup>100</sup> indicating an evolution towards eHDA at 0.1 and 0.2 GPa. The relaxation times  $\tau_R$  obtained from the fitting procedure are extrapolated to slightly higher temperature, where  $\tau_R = 100$  s, in order to locate the glass transition temperature  $T_g$ . We used  $\tau_R(T_g) = 100$  s for the definition of  $T_g$ , a convention used by sev-

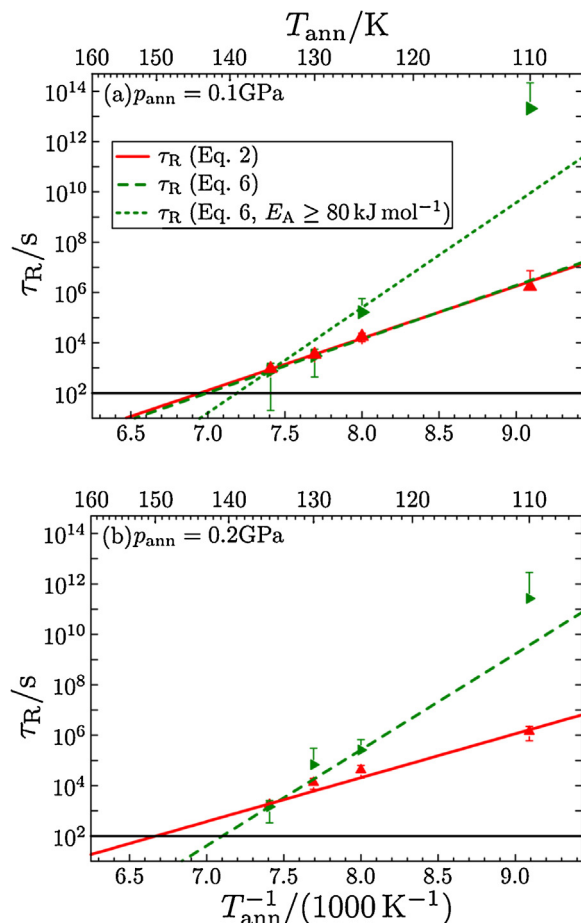


**Fig. 5.** Relaxation times  $\tau_R$  for uHDA<sup>100</sup> samples annealed at 0.1 GPa (a) or 0.2 GPa (b) and the extrapolation according to an Arrhenius fit Eq. (7). Here (▲) mark the relaxation times obtained from the logarithmic fit and (▲) from the relaxation function fit. The dashed lines are the Arrhenius fit of the logarithmic data and the solid lines of the relaxation function data. The dotted line is an Arrhenius fit of the logarithmic fit with restricted activation energy ( $E_A \geq 80 \text{ kJ mol}^{-1}$ ). Please note that the x-axis is scaled as inverse temperature.

eral authors (cf., e.g., Refs. [14,36,51,55,57,58]). The extrapolation is based on an Arrhenius function.

$$\tau_R(T_{\text{ann}}) = \tau_{R,\infty} e^{\frac{E_A}{kT_{\text{ann}}}} \quad (7)$$

The Arrhenius fit yields pre-exponential constants  $\tau_{R,\infty}$  and activation energies  $E_A$ .<sup>2</sup> The use of the Arrhenius function is typically justified for strong liquids (cf., e.g., Ref. [58]) and for glasses themselves (see, e.g., Ref. [51]). It was used here, since we start with a glassy state and since the corresponding liquid is a strong liquid [14]. However, we regard this to be suitable for extrapolation to slightly higher temperature even if the temperature dependence in fact is not Arrhenius. The Arrhenius fits are shown in Fig. 5 for both  $p_{\text{ann}}$ , and all fitting parameters are listed in Table 3.

The activation energies obtained by the relaxation function fit are  $39.6 \text{ kJ mol}^{-1}$  for  $p_{\text{ann}} = 0.1 \text{ GPa}$  and  $33.3 \text{ kJ mol}^{-1}$  for  $p_{\text{ann}} = 0.2 \text{ GPa}$ . The values from the relaxation function are close together and correspond well to the value from the logarithmic fit at  $p_{\text{ann}} = 0.1 \text{ GPa}$ . Also the value of Amann-Winkel et al. [14] obtained from dielectric relaxation at 1 bar of  $34 \text{ kJ mol}^{-1}$  is consistent with the values obtained here. These activation energies for

<sup>2</sup> Please note that for the Arrhenius-fit of the relaxation times the data point obtained for  $p_{\text{ann}} = 0.2 \text{ GPa}$  and  $T_{\text{ann}} = 110 \text{ K}$  via the relaxation function fit with fixed  $T_{e,0}^{\text{H} \rightarrow \text{L}}$  was that point where also  $n$  was fixed (cf. Table 2).

**Table 5**

Crystallization enthalpies of LDA  $\Delta H^{L \rightarrow Lc}$  from literature and an uHDA<sup>100</sup> sample produced here. The specific form of LDA is given. LDA<sub>I</sub> denotes LDA produced via uHDA [61], LDA<sub>II</sub> denotes LDA produced via eHDA [61].

LDA-Subform	$\Delta_{L \rightarrow Lc} H/\text{kJ mol}^{-1}$	Source
LDA <sub>I</sub>	-1.363	[42]
LDA <sub>I</sub>	-1.376	[42]
LDA <sub>I</sub>	-1.425	[42]
LDA <sub>I</sub>	*-1.347	[71]
LDA <sub>II</sub>	-1.32	[61]
LDA <sub>II</sub>	-1.31	[61]
LDA <sub>II</sub>	-1.30	[72]
LDA <sub>I</sub>	-1.269	This work
$\dagger \Delta_{L \rightarrow Lc} H = -1.35 \pm 0.06 \text{ kJ mol}^{-1}$		

\*This value represents a mean of 30 measurements.  $\dagger$ This value was calculated using the 30 individual values from Ref. [71] and the other values given in the table.

**Table 6**

Individual measurement of the HDA  $\rightarrow$  LDA transition enthalpy  $\Delta H^{H \rightarrow L}$  for uHDA<sup>100</sup> samples annealed at 110 K at the annealing pressure  $p_{\text{ann}}$  for the time  $t_{\text{ann}}$ .

$p_{\text{ann}} = 0.1 \text{ GPa}$		$p_{\text{ann}} = 0.2 \text{ GPa}$	
$t_{\text{ann}}/\text{s}$	$\Delta_{H \rightarrow L} H/\text{kJ mol}^{-1}$	$t_{\text{ann}}/\text{s}$	$\Delta_{H \rightarrow L} H/\text{kJ mol}^{-1}$
0	-0.674	0	-0.666
0	-0.653	72	-0.787
76	-0.791	72	-0.820
76	-0.673	198	-0.816
1997	-0.516	198	-0.396
1997	-0.629	2000	-0.783
5969	-0.818	2000	-1.121
5969	-0.675	6002	-0.780
10436	-0.644	6002	-0.721
10436	-0.679	11254	-0.693
-	-	11254	-0.760

relaxation are larger by a factor of 100–200 in comparison to the strain of 200–300 J mol<sup>-1</sup> within the uHDA matrix, again suggesting that strain in uHDA is a factor not significantly speeding up relaxation. The pre-exponential factor  $\tau_{R,\infty}$  is on the order of 10<sup>-13</sup> s at 0.1 GPa and 10<sup>-11</sup> s at 0.2 GPa. This is within the range of the period for OH-stretching vibrations and librational modes of water molecules within the H-bond network. The logarithmic fit produces times about 15 orders of magnitude shorter than that, again demonstrating the unphysical nature of this type of fit. The glass transition temperature  $T_g$  was calculated from the fitted Arrhenius function. The graphic representation of the fit and its extrapolation is depicted in Fig. 5 for both values of  $p_{\text{ann}}$ . Moreover, also the prognosis bands (68.3%) were calculated along with the fit but are not shown in Fig. 5 for clarity. However, the mean deviations of the prognosis bands from the glass transition temperature at  $\tau_R = 100$  s were taken as uncertainty of the respective estimate of glass transition temperature. All calculated values are listed in Table 4. It is noteworthy to recognize that the glass transition temperatures  $T_g$  are relatively insensitive to the type of fit used, and all values agree to within  $\pm 5$  K. That is, they are more robust and afflicted with much less relative error than the relaxation times  $\tau_R$  themselves.

As mentioned above, the quality of the logarithmic fit of the  $T_e^{H \rightarrow L}$  data is clearly inferior. This is again seen when inspecting Fig. 5. First, the data point for  $T_{\text{ann}} = 110$  K and  $p_{\text{ann}} = 0.1$  GPa (Fig. 5(a)) obtained by the logarithmic fit is missed by the Arrhenius fit (dashed line). This is because the uncertainty associated with this data point is particularly high. Second, there is a large discrepancy between the activation energy of 40.9 kJ mol<sup>-1</sup> at 0.1 GPa and 72.9 kJ mol<sup>-1</sup> at 0.2 GPa. We then attempted to fit the data at 0.1 GPa based on the assumption of an activation energy on the order of 80 kJ mol<sup>-1</sup>. The corresponding fit is shown in Fig. 5 (dotted line), with the parameters listed in Table 3. This fit is particularly bad,

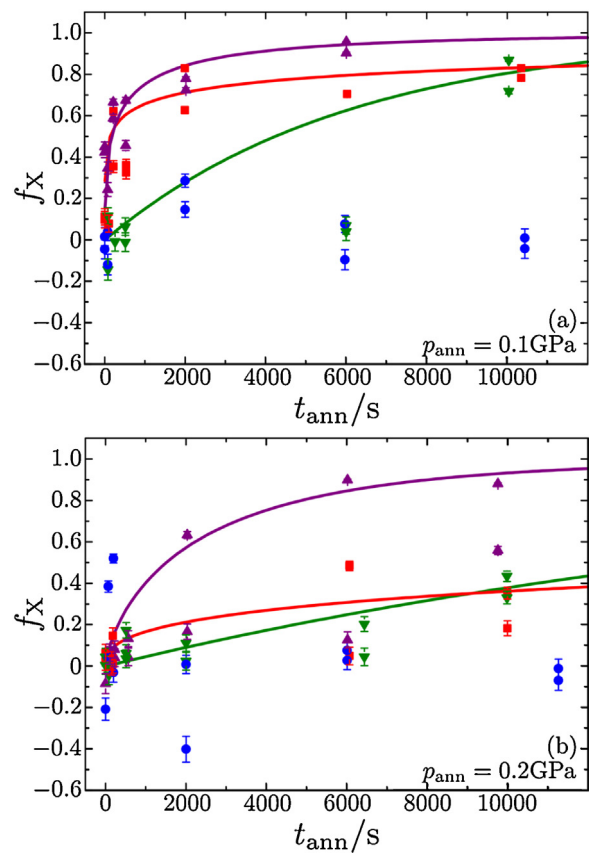


**Fig. 6.** Crystalline fraction  $f_X$  after annealing uHDA<sup>100</sup> at 0.1 GPa or 0.2 GPa and 110 K (●), 125 K (▼), 130 K (■) or 135 K (▲). The corresponding lines show the fits with Eq. (9). In (a) the data point at 5969 s and 125 K was ignored as an outlier.

demonstrating that an activation energy of 70–80 kJ mol<sup>-1</sup> does not describe relaxation of uHDA. In other words, the activation energy of 30–40 kJ mol<sup>-1</sup> obtained from the relaxation function fit is the one we regard to be reliable.

#### 4.3. Analysis of the crystallization enthalpies of LDA

It was recently established that eHDA is much more stable against crystallization than uHDA [46,47], which makes it easier to study the glass transition in eHDA than in uHDA. The fraction of the uHDA sample that crystallizes has to be considered carefully, therefore. As explained above the LDA crystallization enthalpy  $\Delta H^{L \rightarrow Lc}$  decreases with  $t_{\text{ann}}$ . LDA can only be formed via HDA, but not from the crystalline ices encountered in this study. Therefore, the decrease in  $\Delta H^{L \rightarrow Lc}$  indicates an increasing fraction of crystalline material formed from HDA at high pressure. This decrease is observed both at 0.1 GPa and 0.2 GPa at  $T_{\text{ann}} = 125$ –135 K. However,  $\Delta H^{L \rightarrow Lc}$  does not change significantly in samples annealed at  $T_{\text{ann}} = 110$  K even after  $\approx 10$  ks annealing time, i.e., they remain entirely amorphous.

Quantitatively, the crystalline fraction  $f_X$  of the samples can be estimated assuming LDA is well relaxed prior to the transition. This assumption seems justified since the crystallization exotherm is observed well above the glass transition temperature of LDA at 1 bar, 136 K [59,60]. In fact,  $\Delta H^{L \rightarrow Lc}$  is indeed roughly the same for all thermodynamic histories of LDA,  $\Delta H^{L \rightarrow Lc}(\text{LDA}) = -1.35 \pm 0.06 \text{ kJ/mol}$  (cf. Table 5), even when also considering the difference between LDA<sub>I</sub> and LDA<sub>II</sub>, where the latter is regarded as slightly more relaxed form of LDA [61].

**Table 7**

Crystallization kinetics parameters obtained from fitting data in Fig. 6 with Eq. (9).  $\chi^2$ ,  $R^2$  and SSE are statistic measures. For the fit of the dataset at  $p_{\text{ann}} = 0.1 \text{ GPa}$  and  $T_{\text{ann}} = 125 \text{ K}$  the data point at  $t_{\text{ann}} = 5996 \text{ s}$  was ignored as an outlier.

$T_{\text{ann}}/\text{K}$	Restrictions	$\chi^2$	$R^2$	SSE	$\tau_X/\text{s}$	$n$
$p_{\text{ann}} = 0.1 \text{ GPa}$						
125	$\beta \leq 1$	36.7447	0.8756	183.724	$6.1 \times 10^3 \pm 2.3 \times 10^3$	$1.000 \pm 0.724$
130	–	67.2199	0.5675	672.199	$7.3 \times 10^2 \pm 5.1 \times 10^2$	$0.219 \pm 0.080$
135	–	107.3985	0.6773	1073.985	$4.4 \times 10^2 \pm 2.0 \times 10^2$	$0.402 \pm 0.082$
half						
$p_{\text{ann}} = 0.2 \text{ GPa}$						
125	$\beta \leq 1$	5.8712	0.7075	58.712	$2.11 \times 10^4 \pm 7.9 \times 10^3$	$1.000 \pm 0.394$
130	$\beta \leq 1$	16.6268	0.4552	133.014	$7.7 \times 10^4 \pm 1.36 \times 10^5$	$0.392 \pm 0.267$
135	–	101.6633	0.6680	1118.297	$2.51 \times 10^3 \pm 8.2 \times 10^2$	$0.719 \pm 0.231$

**Table 8**

Arrhenius-parameters obtained from fitting the temperature dependence of the relaxation times  $\tau_X(T)$  with Eq. (7).  $\chi^2$ ,  $R^2$  and SSE are statistic measures.

$p_{\text{ann}}/\text{GPa}$	$\chi^2$	$R^2$	SSE	$\tau_{X,\infty}/\text{s}$	$E_A/\text{kJ mol}^{-1}$
0.1	1.3879	0.5715	1.3879	$6.6 \times 10^{-14} \pm 7.23 \times 10^{-13}$	$40.4 \pm 10.7$
0.2	0.2617	0.9073	0.2617	$7.5 \times 10^{-9} \pm 2.30 \times 10^{-8}$	$29.8 \pm 3.1$

For comparison, in case of annealed vapour-deposited amorphous solid water (ASW)  $\Delta H^{L \rightarrow Ic}(\text{ASW}) = -1.29 \pm 0.01 \text{ kJ/mol}$  [62] and in case of annealed hyperquenched glassy water (HGW)  $\Delta H^{L \rightarrow Ic}(\text{HGW}) = -1.43 \pm 0.03 \text{ kJ/mol}$  [63]. In case of unannealed hyperquenched water, astonishingly, a lower value  $\Delta H^{L \rightarrow Ic}(\text{HGW}) = -1.33 \pm 0.02 \text{ kJ/mol}$  [63] was reported and explained on the basis of enthalpy relaxation causing a sloping baseline. Since LDA, ASW and HGW are all considered to represent the glassy state connected to the same low-density liquid LDL [24,60], the difference between these values represents the error-bar of the DSC determination of  $\Delta_{L \rightarrow Ic}H$ , which is  $\pm 5\%$ . In other words, based on this approach the crystalline fraction cannot be determined to better than  $\pm 5\%$  from  $\Delta H^{L \rightarrow Ic}$ .

To calculate  $f_X$  from  $\Delta_{L \rightarrow Ic}H$  the following relation was used:

$$f_X(t_{\text{ann}}) = 1 - \frac{\Delta H^{L \rightarrow Ic}(t_{\text{ann}})}{\Delta H^{L \rightarrow Ic}(\text{LDA})} \quad (8)$$

Here  $\Delta H^{L \rightarrow Ic}(t_{\text{ann}})$  denotes the measured crystallization enthalpy of LDA in annealed uHDA<sup>100</sup> samples and  $\Delta H^{L \rightarrow Ic}(\text{LDA})$  denotes the reference crystallization enthalpy of pure LDA. As reference value the mean value of the enthalpy of the  $\text{LDA} \rightarrow \text{I}_c$  transition of own uHDA<sup>100</sup> samples produced here and values for LDA<sub>I</sub> and LDA<sub>II</sub> from literature were used (see Table 5). The crystalline fraction of ice<sub>X</sub> in the course of our annealing experiments is shown in Fig. 6, where error-bars on  $f_X$  were calculated via Gaussian error progression. Unphysical negative values are a result of the uncertainty in  $\Delta H^{L \rightarrow Ic}$  mentioned above in combination with the statistical error on the individual measurements. In such cases absence of crystallinity was assumed, i.e.,  $f_X = 0$ . The error also includes the possibility that the crystalline fraction is not homogeneously distributed in the sample, i.e., there may be sample chips with less and chips with more crystallinity. Therefore, the following quantitative evaluation needs to be taken with care and to be understood as a rough estimate – overestimation as well as underestimation of the crystalline amount is possible. Nevertheless, the trends in these data are quite clear and as expected – crystalline fraction increases with annealing time  $t_{\text{ann}}$ , and higher annealing temperatures  $T_{\text{ann}}$  result in faster crystallization. No crystallization was observed for samples annealed at  $T_{\text{ann}} = 110 \text{ K}$  at the timescale of  $\approx 10 \text{ ks}$ . Due to this fact also the molar enthalpies of the  $\text{HDA} \rightarrow \text{LDA}$  transition  $\Delta H^{H \rightarrow L}$  can be directly compared in Table 6, without disturbing influence of crystallinity. At  $T_{\text{ann}} = 110 \text{ K}$   $\Delta H^{H \rightarrow L}$  does not decrease significantly, i.e., enthalpy relaxation is not detected on the timescale 10 ks. Anyhow, the onset temperatures showed a slight increase after  $\approx 10 \text{ s}$  (cf. Fig. 4).

#### 4.3.1. Fit of the temperature dependence of the crystalline fraction

Based on the dependence of  $f_X$  on  $t_{\text{ann}}$  shown in Fig. 6 it is possible to extract a characteristic crystallization time  $\tau_X$ , similar to the relaxation time  $\tau_R$ . To this end we use a function analogous to Eq. (6), but with different boundary conditions for the maximum ( $f_X(\infty) = 1$ ) and minimum ( $f_X(0) = 0$ ):

$$f_X(t) = 1 - e^{-\left(\frac{t}{\tau_X}\right)^n} \quad (9)$$

Here  $\tau_X$  and  $n$  served as fitting parameters. The fits were done using OriginPro 8 G for data sets with  $T_{\text{ann}} > 110 \text{ K}$ , since no crystallization was observed for samples annealed at 110 K. The data point  $t_{\text{ann}} = 5996 \text{ s}$  at  $p_{\text{ann}} = 0.1 \text{ GPa}$  and  $T_{\text{ann}} = 125 \text{ K}$  was regarded to be an outlier and ignored in the fit. All fits are shown in Fig. 6. The resulting crystallization times are summarized in Table 7 alongside all other parameters and are plotted in Fig. 7(a) and (c). Fig. 7(b) and (d) compare the Arrhenius fits for  $\tau_X$ .<sup>3</sup> The Arrhenius parameters summarized in Table 8 indicate activation energies for crystallization of  $30\text{--}40 \text{ kJ mol}^{-1}$  and pre-factors on the order of  $10^{-14}\text{--}10^{-10} \text{ s}$ . These are strikingly similar to the Arrhenius parameters describing relaxation, as is also evident from Fig. 5. More precisely, the  $\tau_X$  curves are the leftmost curves especially at low temperatures. This implies that at low temperatures crystallization is faster than the relaxation. Partial crystallization is, therefore, already observed when the samples are heated to the desired  $T_{\text{ann}}$ , in accord with the gradual crystallization observed by Salzmann et al. [45], Seidl et al. [46,47] and the XRD measurements presented here (see Fig. 3(b)). However, also the relaxation is accessible, since the timescales are very similar. At 0.2 GPa our estimates even indicate that the relaxation is faster than the crystallization at temperatures above  $\approx 125 \text{ K}$ . This behaviour is also reflected in the activation energies, which are very similar for relaxation and crystallization (see Tables 3 and 7). From the obtained parameters also the crystallization time at 110 K can be calculated. It is  $\approx 1 \times 10^6 \text{ s}$  for both pressures. These values are consistent with the apparent absence of crystallization at the studied timescale of  $\approx 10 \text{ ks}$  at this temperature.

In Fig. 7 also the crystallization times from Ref. [64] are shown for comparison. These  $\tau_X$  were obtained for VHDA at 0.1 GPa (shown in part (b)) and 0.25 GPa (shown in part (d)). Interestingly these curves are different from the  $\tau_X$  of uHDA<sup>100</sup>. In particular, VHDA crystallizes slower than uHDA, such that the curve is shifted by

<sup>3</sup> Please note that in comparison to Eq. (7)  $\tau_X$  and  $\tau_{X,\infty}$  have been used instead of  $\tau_R$  and  $\tau_{R,\infty}$ .

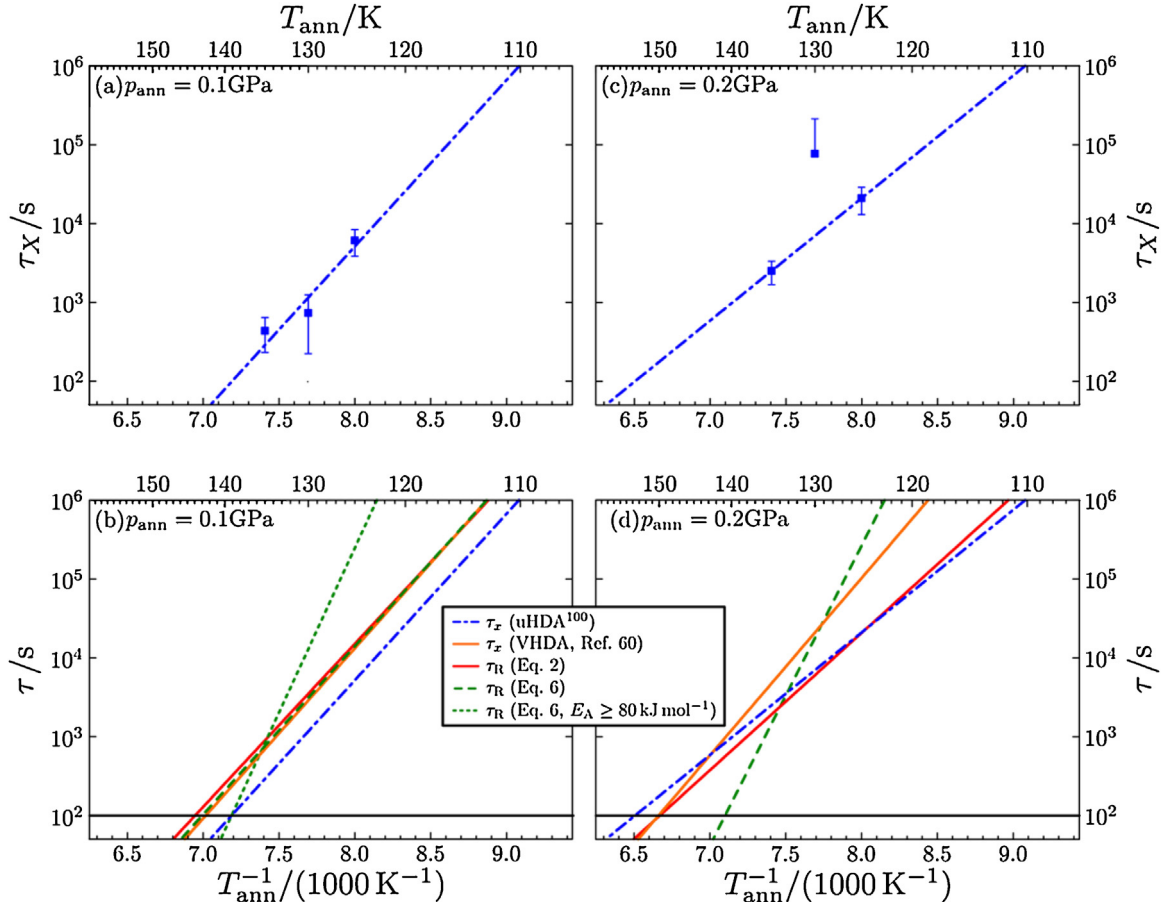


**Fig. 7.** Crystallization times  $\tau_X$  (■) for uHDA<sup>100</sup> samples annealed at 0.1 GPa (a) and 0.2 GPa (c). The dash-dotted lines are Arrhenius fits Eq. (7). In (b) and (d)  $\tau_X(T)$  (blue, dash-dotted line) is compared with  $\tau_R(T)$  from Fig. 5(a) and (b) (green line and red line). Also the crystallization times  $\tau_X$  of VHDA at 0.1 GPa (b) and at 0.25 GPa (d) are shown as orange lines. Those values are the inverse ( $\tau_X = k_X^{-1}$ ) of the respective rate constants of crystallization  $k_X$  shown in Ref. [64]. Please note that the x-axis is scaled as inverse temperature. (For interpretation of the references to color in this figure legend, the reader is referred to the web version of this article.)

about 3 K to higher temperatures for VHDA at 0.10 GPa. Still one has to be careful interpreting this small effect considering the uncertainties of the crystallization times of uHDA. Nevertheless, we believe this to indicate that VHDA crystallizes differently than uHDA, a fact that was already pointed out for eHDA [46,47]. Furthermore, the VHDA crystallization is practically identical with the relaxation time of amorphous ice (compare orange and red curves in Fig. 7(b)). We surmise relaxation of the amorphous matrix to lower densities has to precede crystallization in VHDA since the crystallizing ice phases are of a density similar to uHDA, but 10% lower in density compared to VHDA. Density relaxation preceding crystallization suggests that the (slow) relaxation rather than (fast) crystallization is the time limiting step for VHDA crystallization at low pressures of <0.3 GPa.

## 5. Summary

We here expand on our earlier work [13] on the isobaric-isothermal relaxation of uHDA<sup>100</sup> at 0.1 and 0.2 GPa as a function of time and temperature. Our *ex situ* strategy of obtaining relaxation times  $\tau_R$  and the interpretation of our observations was recently assessed and questioned by Johari [31]. Here we reply to the criticism, describe all our measurement and data analysis procedures in detail and present additional data to reconfirm our earlier interpretation and conclusions. We explain why the relaxation of the amorphous matrix can be observed best on the basis of the shift of the calorimetric onset temperature of the HDA → LDA transition at ambient pressure. The shift in this transition temperature was

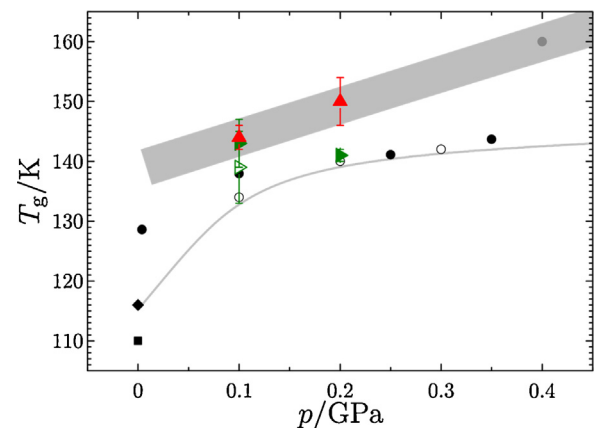


**Fig. 8.** Glass transition temperatures  $T_g$  obtained from the logarithmic fit (►), the restricted logarithmic fit (▷) and the relaxation function fit (▲) in comparison with data from literature. Data published in 2012 (Ref. [13]) are the same as (▲). The only difference is the error bar at 0.2 GPa (cf. Ref. [13]). Other data points are from Ref. [14] (eHDA, DSC,  $q = 10 \text{ K min}^{-1}$ , ■; eHDA, dielectric spectroscopy,  $q \approx 0.01 \text{ K min}^{-1}$ , ♦), Ref. [12] (eHDA, high-pressure volumetry,  $q = 2 \text{ K min}^{-1}$ , ○), Ref. [9] (VHDA,  $T$ -change during decompression at 160 K with 0.2 GPa min<sup>-1</sup>, ●) and Ref. [70] (Solid gray line, prediction from the ST2 water model for HDA).

fitted by two different models, a logarithmic fit and a relaxation function fit, yielding relaxation times  $\tau_R$ . The relaxation times drop dramatically from 110 K to 135 K at both pressures. We regard  $\tau_R$  to be a good estimate for  $\tau_\alpha$  and the differences to be insignificant. From the observed temperature dependence of  $\tau_R$  the glass transition temperatures  $T_g$  could be estimated by extrapolating to  $\tau_R = 100$  s using Arrhenius fits. These  $T_g$ s are summarized in Table 4 and compared with literature data in Fig. 8. The extrapolated  $T_g$  values compare well to the literature values, in spite of the strained nature of uHDA<sup>100</sup>. On basis of the statistical measures the fit with the relaxation function seems to be the better choice. This fit yields glass transition temperatures for HDA of about  $144 \pm 1$  K for 0.1 GPa and  $150 \pm 4$  K for 0.2 GPa. Use of the decrease in the transition enthalpy to monitor the degree of relaxation in the HDA sample would be desirable, but is impaired by crystallization occurring in parallel to relaxation.

Furthermore, we report rough estimates of the crystallization times  $\tau_X$  between 125 K and 135 K at 0.1 GPa and 0.2 GPa uHDA<sup>100</sup> samples at 0.1 and 0.2 GPa relax at similar timescales as they crystallize. Nevertheless, it is possible to significantly relax uHDA at 0.1 and 0.2 GPa prior to its full crystallization, although both processes are competitive and contribute to the phenomenology, i.e., uHDA samples simultaneously crystallize and relax at 0.1 GPa and 0.2 GPa. By comparison, eHDA crystallizes much slower in this pressure range [47], which makes it easier to study the glass transition in eHDA than in uHDA.

## Acknowledgments

We gratefully acknowledge scientific discussion with Roland Böhmer and Franz Fujara. We are thankful for financial support by the Austrian Science Fund FWF (Erwin Schrödinger Fellowship No. J3811 N34 to P.H.H. and project I1392 to T.L.). V.F.L. and M.S. are recipients of a DOC Fellowship of the Austrian Academy of Sciences ÖAW at the Institute of Physical Chemistry, University of Innsbruck.

## References

- [1] M. Chaplin, <<http://www1.lsbu.ac.uk/water/>>, (accessed 08.05.16).
- [2] P.G. Debenedetti, *J. Phys.: Condens. Matter* 15 (2003) R1669.
- [3] P.H. Poole, F. Sciortino, U. Essmann, H.E. Stanley, *Nature* 360 (1992) 324.
- [4] O. Mishima, *Nature* 384 (1996) 546.
- [5] O. Mishima, L.D. Calvert, E. Whalley, *Nature* 310 (1984) 393.
- [6] O. Mishima, Y. Suzuki, *J. Chem. Phys.* 115 (2001) 4199.
- [7] S. Klotz, G. Hamel, J.S. Loveday, R.J. Nelmes, M. Guthrie, A.K. Soper, *Phys. Rev. Lett.* 89 (2002) 285502.
- [8] S. Klotz, G. Hamel, J.S. Loveday, R.J. Nelmes, M. Guthrie, *Z. Kristallogr.* 218 (2003) 117.
- [9] O. Mishima, *J. Chem. Phys.* 121 (2004) 3161.
- [10] S. Klotz, T. Straessle, A.M. Saitta, G. Rousse, G. Hamel, R.J. Nelmes, J.S. Loveday, M. Guthrie, *J. Phys.: Cond. Matter* 17 (2005) S967.
- [11] Y. Suzuki, Y. Tominaga, *J. Chem. Phys.* 133 (2010) 164508.
- [12] M. Seidl, M.S. Elsaesser, K. Winkel, G. Zifferer, E. Mayer, T. Loerting, *Phys. Rev. B* 83 (2011) 100201.
- [13] P.H. Handle, M. Seidl, T. Loerting, *Phys. Rev. Lett.* 108 (2012) 225901.
- [14] K. Amann-Winkel, C. Gainaru, P.H. Handle, M. Seidl, H. Nelson, R. Böhmer, T. Loerting, *Proc. Natl. Acad. Sci. U. S. A.* 110 (2013) 17720.
- [15] A.I. Kolesnikov, V.V. Sinitsyn, E.G. Pomyatovsky, I. Nathkaniec, L.S. Smirnov, *Physica B* 213 (1995) 474.
- [16] H. Schober, M. Koza, A. Tölle, F. Fujara, C.A. Angell, R. Böhmer, *Physica B* 241–243 (1998) 897.
- [17] J.S. Tse, D.D. Klug, C.A. Tulk, I. Swainson, E.C. Svensson, C.K. Loong, V. Shpakov, V.R. Belosludov, R.V. Belosludov, Y. Kawazoe, *Nature* 400 (1999) 647.
- [18] G.P. Johari, *Phys. Chem. Chem. Phys.* 2 (2000) 1567.
- [19] H. Schober, M.M. Koza, A. Tolle, C. Masciovecchio, F. Sette, F. Fujara, *Phys. Rev. Lett.* 85 (2000) 4100.
- [20] M.M. Koza, B. Geil, K. Winkel, C. Koehler, F. Czeschka, M. Scheuermann, H. Schober, T. Hansen, *Phys. Rev. Lett.* 94 (2005) 125506.
- [21] M.M. Koza, T. Hansen, R.P. May, H. Schober, *J. Non-Cryst. Solids* 352 (2006) 4988.
- [22] M.M. Koza, R.P. May, H. Schober, *J. Appl. Cryst.* 40 (2007) s517.
- [23] M.M. Koza, B. Geil, M. Scheuermann, H. Schober, G. Monaco, H. Requardt, *Phys. Rev. B* 78 (2008) 224301.
- [24] T. Loerting, K. Winkel, M. Seidl, M. Bauer, C. Mitterdorfer, P.H. Handle, C.G. Salzmann, E. Mayer, J.L. Finney, D.T. Bowron, *Phys. Chem. Chem. Phys.* 13 (2011) 8783.
- [25] R.J. Nelmes, J.S. Loveday, T. Straessle, C.L. Bull, M. Guthrie, G. Hamel, S. Klotz, *Nat. Phys.* 2 (2006) 414.
- [26] T. Loerting, C. Salzmann, I. Kohl, E. Mayer, A. Hallbrucker, *Phys. Chem. Chem. Phys.* 3 (2001) 5355.
- [27] K. Winkel, M.S. Elsaesser, E. Mayer, T. Loerting, *J. Chem. Phys.* 128 (2008) 044510.
- [28] K. Winkel, M.S. Elsaesser, M. Seidl, M. Bauer, E. Mayer, T. Loerting, *J. Phys.: Condens. Matter* 20 (2008) 494212.
- [29] K. Winkel, E. Mayer, T. Loerting, *J. Phys. Chem. B* 115 (2011) 14141.
- [30] C.G. Salzmann, T. Loerting, S. Klotz, P.W. Mirwald, A. Hallbrucker, E. Mayer, *Phys. Chem. Chem. Phys.* 8 (2006) 386.
- [31] G.P. Johari, *Thermochim. Acta* 589 (2014) 76.
- [32] J. Stern, M. Seidl, C. Gainaru, V. Fuentes-Landete, K. Amann-Winkel, P.H. Handle, K.W. Koester, H. Nelson, R. Boehmer, T. Loerting, *Thermochim. Acta* 617 (2015) 200.
- [33] G.P. Johari, *Thermochim. Acta* 617 (2015) 208.
- [34] T.L. Malkin, B.J. Murray, C.G. Salzmann, V. Molinero, S.J. Pickering, T.F. Whale, *Phys. Chem. Chem. Phys.* 17 (2015) 60.
- [35] T.C. Hansen, C. Sippel, W.F. Kuhs, *Z. Kristallogr.* 230 (2015) 75.
- [36] P.G. Debenedetti, F.H. Stillinger, *Nature* 410 (2001) 259.
- [37] K. Winkel, *Study of Amorphous–Amorphous Transitions in Water*, Verlag Dr. Hut, Munich, 2011.
- [38] T. Loerting, V.V. Brazhkin, T. Morishita, *Adv. Chem. Phys.* 143 (2009) 29.
- [39] T. Loerting, V. Fuentes-Landete, P.H. Handle, M. Seidl, K. Amann-Winkel, C. Gainaru, R. Böhmer, *J. Non-Cryst. Solids* 407 (2015) 423.
- [40] K. Amann-Winkel, R. Böhmer, F. Fujara, C. Gainaru, B. Geil, T. Loerting, *Rev. Mod. Phys.* 88 (2016) 011002.
- [41] O. Mishima, L.D. Calvert, E. Whalley, *Nature* 314 (1985) 76.
- [42] Y.P. Handa, O. Mishima, E. Whalley, *J. Chem. Phys.* 84 (1986) 2766.
- [43] H.R. Pruppacher, J.D. Klett, *Microphysics of Clouds and Precipitation*, D. Reidel, Dordrecht, 1980.
- [44] G. Höhne, W.F. Hemminger, H.-J. Flammersheim, *Differential Scanning Calorimetry*, second ed., Springer Verlag, 2003.
- [45] C.G. Salzmann, E. Mayer, A. Hallbrucker, *Phys. Chem. Chem. Phys.* 6 (2004) 5156.
- [46] M. Seidl, K. Amann-Winkel, P.H. Handle, G. Zifferer, T. Loerting, *Phys. Rev. B* 88 (2013) 174105.
- [47] M. Seidl, A. Fayter, J.N. Stern, G. Zifferer, T. Loerting, *Phys. Rev. B* 91 (2015) 144201.
- [48] M.M. Koza, H. Schober, H.E. Fischer, T. Hansen, F. Fujara, *J. Phys.: Condens. Matter* 15 (2003) 321.
- [49] V.G. Karpov, M. Grimsditch, *Phys. Rev. B: Condens. Matter* 48 (1993) 6941.
- [50] C.T. Moynihan, *Rev. Mineral.* 32 (1995) 1.
- [51] I.M. Hodge, *J. Non-Cryst. Solids* 169 (1994) 211.
- [52] P.H. Handle, Ph.D. Thesis, University of Innsbruck, 2015.
- [53] F. Löw, K. Amann-Winkel, B. Geil, T. Loerting, C. Wittich, F. Fujara, *Phys. Chem. Chem. Phys.* 15 (2013) 576.
- [54] O. Andersson, *Phys. Rev. Lett.* 95 (2005) 205503.
- [55] O. Andersson, A. Inaba, *Phys. Rev. B* 74 (2006) 184201.
- [56] O. Andersson, *J. Phys. Condens. Matter* 20 (2008) 244115.
- [57] C.A. Angell, K.L. Ngai, G.B. McKenna, P.F. McMillan, S.W. Martin, *J. Appl. Phys.* 88 (2000) 3113.
- [58] M.I. Ojovan, *Adv. Condens. Matter Phys.* 2008 (2008) 817829.
- [59] S. Capaccioli, K.L. Ngai, *J. Chem. Phys.* 135 (2011) 104504.
- [60] N. Giovambattista, K. Amann-Winkel, T. Loerting, *Adv. Chem. Phys.* 152 (2013) 139.
- [61] K. Winkel, D.T. Bowron, T. Loerting, E. Mayer, J.L. Finney, *J. Chem. Phys.* 130 (2009) 204502.
- [62] A. Hallbrucker, E. Mayer, G.P. Johari, *J. Phys. Chem.* 93 (1989) 4986.
- [63] G.P. Johari, A. Hallbrucker, E. Mayer, *J. Chem. Phys.* 92 (1990) 6742.
- [64] P.H. Handle, T. Loerting, *Phys. Rev. B* 93 (2016) 064204.
- [65] M. Seidl, A. Fayter, J.N. Stern, K. Amann-Winkel, M. Bauer, T. Loerting, *Proceedings of the 6th Zwick Academia Day 2015*, Zwick GmbH & Co. KG, Ulm, 2015.
- [66] W.F. Kuhs, M.S. Lehmann, in: F. Franks (Ed.), *Water Science Reviews* 2, vol. 1, Cambridge University Press, Cambridge, 1986.
- [67] K. Röttger, A. Endriss, J. Ihringer, S. Doyle, W.F. Kuhs, *Acta Crystallogr. B50* (1994) 644.
- [68] V.F. Petrenko, R.W. Whitworth, *Physics of Ice*, Oxford University Press, Oxford, 1999.
- [69] H.E. Swanson, Standard x-ray diffraction powder patterns, U.S. Dept. of Commerce, National Bureau of Standards: For sale by the Supt. of Docs., U.S. G.P.O., Washington, DC, 1953.
- [70] N. Giovambattista, T. Loerting, B.R. Lukanov, F.W. Starr, *Sci. Rep.* 2 (2012) 390.
- [71] I. Kohl, Ph.D Thesis, University of Innsbruck, Innsbruck, 2001.
- [72] M.S. Elsaesser, K. Winkel, E. Mayer, T. Loerting, *Phys. Chem. Chem. Phys.* 12 (2010) 708.